Modeling Microtopographic Effects in Watershed-scale Integrated Surface/Subsurface Models

Abstract

In permafrost-affected regions, subsurface is mainly characterized by ice-wedge polygons and manifests a patterned polygonal ground. The role of patterned polygonal ground and associated fine-scale microtopography (spatial heterogeneities at a scale smaller than the size of polygons) in controlling surface/subsurface thermal hydrology is critical but well-understood. Fine-scale simulations are required to capture microtopographic influences on flow. Standalone fine-scale surface hydrology simulations are feasible with modern computing tools. However, highly resolved integrated surface/subsurface thermal hydrology simulations are not tractable at watershed scale and requires proper modeling. To capture the effects of microtopographic features (such as depressions, obstructions etc.) in coarsened model, we present a subgrid model parameterized by small-scale spatial heterogeneities. The subgrid model alters the water storage and flow terms in the existing governing equations. We demonstrate how a few parameters extracted from the available fine-scale information can be utilized to account for microtopographic effects in coarsened watershed-scale integrated models. Simulations were carried out and numerical results of the subgrid model were compared both to those generated with no subgrid model and to fine-scale results of seven ice-wedge polygons. Our findings confirm that the subgrid model improves the shape of the hydrographs and the to-

tal water content in the system, and that the results are very close to the corresponding fine-scale simulations. Watershed-scale fully integrated surface/subsurface simulations with the subgrid model show that the surface depressions increase infiltration and reduce runoff, thereby highlighting the importance of microtopographic effects on the watershed-scale hydrology.
Keywords: Subgrid model, Polygonal tundra, Microtopography, Watershed, Integrated Surface/Subsurface

1. Introduction

To better understand the interactions between surface and subsurface, surface runoff and discharge rate, it is important to gain insight into the role of heterogeneous spatial structure of the ground surface. It is well understood that spatial heterogeneities in the surface microtopography (unevenness at small scale) serve a critical role in surface water retention, surface/subsurface interactions, delay runoff, and thereby significantly affects the shape of hydrographs [4, 1, 2][**References**]. In general, an accurate flow representation is achieved at fine-scale (a scale of centimeters) and fortunately with the availability of sophisticated simulation tools, standalone highly resolved surface-flow simulations are easily tractable. However, fully integrated surface/subsurface thermal hydrology simulations with highly resolved computational grid are not tractable at watershed scale. That said, if the microtopographic effects are ignored in the integrated models, the processes representing flow will not be completely accurate. The idea to incorporate fine-scale flow behavior in the watershed-scale integrated models motivates the use of subgrid representation. A subgrid model is build on the information gained from highly resolved surface topographic data:

the depressions and obstructions. Depressions are disconnected low points in the topography (surface pits) that retain water that is available only for infiltration or/and evaporation. Obstructions are objects exit above the depressions that interrupt and slow the flow, but do not completely block it. It is worth to point out, that we intend to use the subgrid parametrization with a mixed-dimensional model reported here [3], where the subsurface is discretized as independent columns and coupled through a surface flow system. In this work, the subgrid parameterization is applied to the lateral flow part only, which is the surface system. This is one aspect of incorporating the microtopographic effects in watershed-scale integrated models, however, in general, both the surface and subsurface require a subgrid model. In this work, we are testing a hypothesis that the effects of microtopography can be captured in coarsened models through the use of a subgrid model. We evaluate one possible form of that model, and explore how parameters can be deduced from the available information.

Here we use polygonal tundra as an example. Low-relief Arctic landscapes exhibit patterned polygonal ground developed by repeated freezing and thawing of ground soil. Thawing ice-wedge polygons lead to a complex mosaic of topographic patterns – heterogeneity at and below the scale of the size of polygon. We call spatial scale variability in the topography at and below the scale of the size of polygon as macro- and micro-topography, respectively. Small scale features of the polygonal landscapes can have regional impacts on hydrology, active-layer thickness and permafrost degradation. Thereby, simulating permafrost soils at a scale of macrotopography (or larger) could lead to an inaccurate estimate of carbon release and energy balance etc. under warming trends in the Arctic landscapes; for example see [4, 2, 19]. More details are provided in section 2.

Pertinent to the literature, integrated suface/subsurface modeling has received considerable attention from researchers across the world; see, for example, [5, 6, 7] and references therein. Here we focus only on the subgrid modeling approach. Though the concept of microtopographic features and their implications on the flow and discharge is not new, but has not been fully addressed and understood from modeling perspective. In the mid-1950s, the significance of the surface microtopographic features were described in [8]. A one-dimensional simulations to study the effects of spatially varying surface roughness on flow hydrographs is presented in [1]. Panday and Huyakorn (2004) presented an integrated surface/subsurface flow model with subgrid representation through the surface depressions and obstructions by modifying the overland flow governing equation. **INCOMPLETE!!**

The rest of the paper is organized as follows. Section 2 introduces the Arctic patterned polygonal ground. Section 3.2 presents the derivation of the governing equations of the subgrid model. A short description, for a quick reference, of the Advanced Terrestrial Simulator (ATS) and the Arcos multiphysics management framework, within which we implemented our subgrid model, is presented in Section 4. In Section 5 we compare the numerical results of our subgrid model with no subgrid model and fine-scale results to illustrate the accuracy of our subgrid model for capturing fine-scale microtopographic features. Finally, in Section 6, we offer closing remarks and future research inline with thaw-induced subsidence.

2. Field Site: Arctic Patterned Polygonal Ground

A large amount of frozen organic carbon is stored in permafrost-affected soils of the Northern Hemisphere [10, 11]. The ground in the Arctic regions

is temperature-sensitive and under potential risk of carbon release to the atmosphere in a changing climate [12]. Arctic landscapes are dominated by polygonal patterned (interconnected polygons) ground. The formation of polygonal landscapes in permafrost-affected regions is a consequence of recurring cracks-compression process over hundreds of thousands of years. During winter, vertical fractures are formed due to ground contraction, the water from the snowmelt in the following summer penetrates those cracks and refreezes. In the following winter, the reexpansion of the ice in the cracks compresses the soil horizontally. The recurring crack-compression process over long period of time develops wedges of ice and finally a polygonal landscape is formed [13, 14, 15, 16]. Figure 1 displays a polygonal tundra, a field site of the U.S. Department of Energy's Next Generation Ecosystem Experiments (NGEE) Arctic project located within the Barrow Environmental Observatory (BEO) [17]. Several types of polygons are formed due to permafrost degradation. Typically, the polygons are classified as low-centered polygon (LCP) and high-centered polygon (HCP) based on surface microtopography. The LCP has a raised rim and central depression, thereby holds ponded water in the center during the summer that can only be available for infiltration and evaporation. The HCP has elevated center that slopes downward to trough and enhances runoff, thus the center may remain mostly dry. Thawing of ice-wedges causes the raised rims of LCP to subside that leads to the formation of HCP [18]. The loss of depression storage in the LCP has the ability to connect the disconnected troughs, thus transforms a poorly drained tundra to a well-established drainage network. Those changes will potentially alter the entire ecosystem and will bring substantial hydrological changes (e.g., surface/subsurface interactions, distribution of surface water, discharge rate etc.) [19, 12, 20, 21].

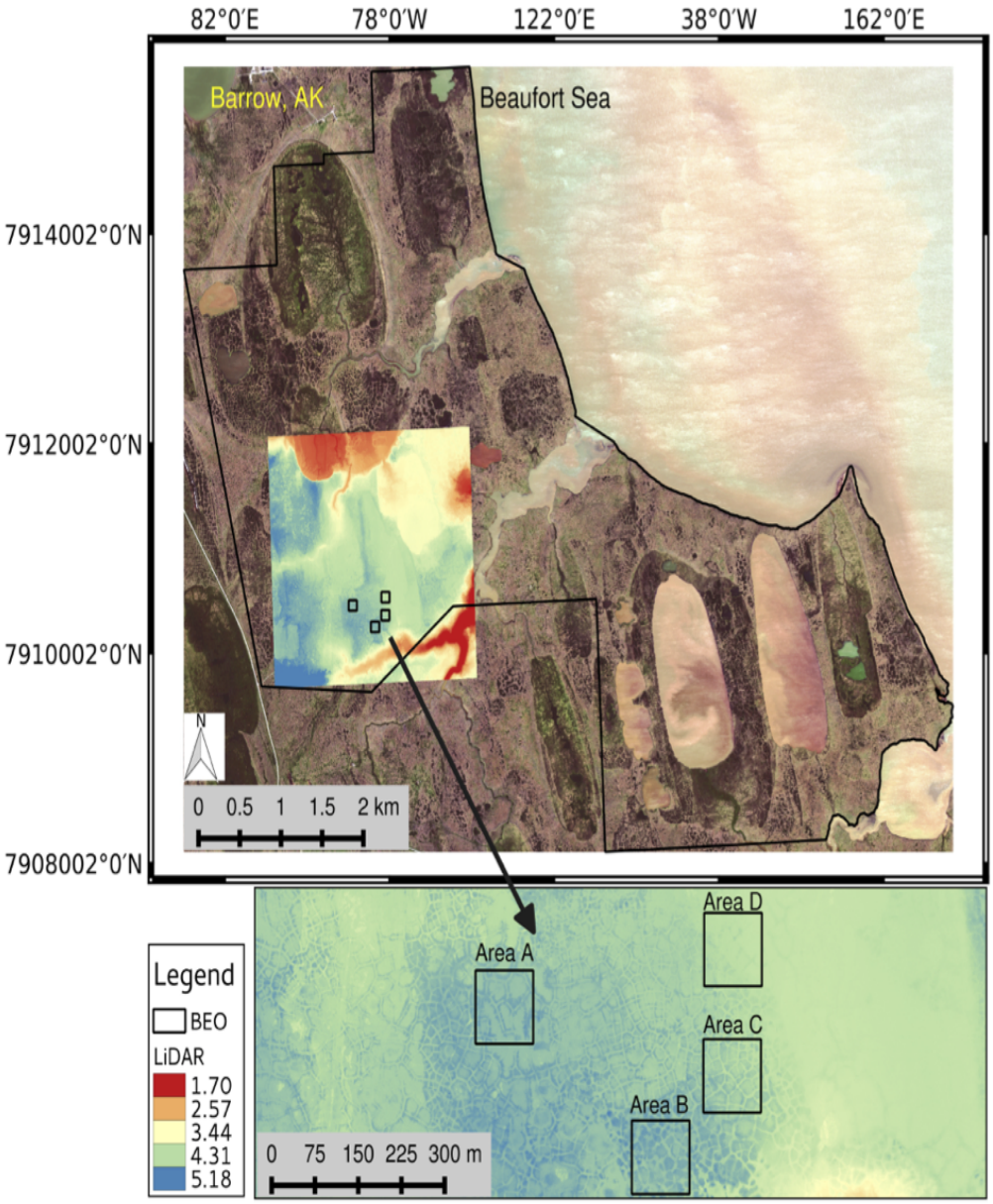

Figure 1: NGEE-Arctic field sites at BEO [17].

3. Surface Flow Model

This section describes diffusion wave equation for surface flow representation. In this work, we will be referring to three types of models as follow:

I. (Fine-scale model) Diffusion wave equation with high-resolved mesh. Grid size at a scale of centimeters.

II. (No subgrid model) Diffusion wave equation with coarsened mesh. Grid size at a scale of meters.

III. (Subgrid model) Modified diffusion wave equation (derived in subsection 3.2) with coarsened mesh. Grid size at a scale of meters.

3.1. Diffusion Wave Equation

Diffusion wave equation for surface flow representation is given by,

$$\frac{\partial \delta}{\partial t} + \nabla \cdot (\delta V) = q_{\mathrm{rp}} + \Gamma_{\mathrm{ex}}. \tag{1}$$

Here δ represents ponded depth, q_{rp} is rain precipitation rate, Γ_{ex} is water exchange between surface and subsurface systems, t is time, and V denotes surface flow velocity given by,

$$V = -\frac{\delta^{2/3}}{n_{\mathrm{man}}(\|\nabla z\| + \epsilon)^{1/2}} \nabla(z + \delta), \tag{2}$$

where n_{man} is Manning's coefficient, z is surface elevation, and $\epsilon > 0$ is a regularization parameter to avoid zero bed slope. More details about the models implemented in ATS can be found here [7]. Units are provided in Table 1.

Table 1: Physical quantities with units

Physical quantities	SI units
Ponded depth (δ)	m
Elevation (z)	m
Rain precipitation rate (q_{rp})	$\mathrm{m}^3/(\mathrm{m}^2\ \mathrm{s})$
Exchange term (Γ_{ex})	$\mathrm{m}^3/(\mathrm{m}^2\ \mathrm{s})$
Manning's coefficient (n_{man})	$\mathrm{m}^{-1/3}\ \mathrm{s}$
Time (t)	s

3.2. Subgrid Model

Subgrid model incorporates depressions and obstructions in coarsened models to capture microtopgraphic effects on flow. It requires to alter accumulation term and flow law in the diffusion wave equation given by Equation 1. For example, the ponded depth (δ) in the accumulation term is typically replaced with a volumetric depth ($\Phi(\delta)$) given by Equation 4, the ponded depth that would occur if the surface were flat. A modified flow velocity is introduced to account for depressions and obstructions given by Equation 5.

3.2.1. Derivation of Volumetric Depth

The volumetric head may be calculated on geometric arguments. Specifically, if the microtopographic elevation field on an ice-wedge polygon (IWP) is $Z_*(x, y)$, the the volumetric depth is

$$\Phi(\delta) = \frac{1}{A} \iint \left(\delta + Z_0 - Z_*(x,y)\right) H\left(\delta + Z_0 - Z_*(x,y)\right) dxdy. \qquad (3)$$

Where the integration is over the surface of the IWP, A is the area of the IWP, Z_0 is the minimum elevation in the IWP, and H is the Heaviside

function. This could be computed from the microtopography and stored as a lookup table. Or, we could employ a simpler parameterization. To that end, we consider parameterizing the microtopography with two parameters: (1) the elevation range spanned by the subgrid microtopography $\delta_{\max}$, and (2) the specific excluded volume δ_{ex}, which is the soil volume per unit bulk area. Then, we approximate the volumetric depth as

$$\Phi(\delta) = \begin{cases} (2\delta_{\max} - 3\delta_{\text{ex}}) \left(\frac{\delta}{\delta_{\max}}\right)^2 + (2\delta_{\text{ex}} - \delta_{\max}) \left(\frac{\delta}{\delta_{\max}}\right)^3 & \text{if } \ 0 \leq \delta \leq \delta_{\max}, \\ \delta - \delta_{\text{ex}} & \text{if } \ \delta > \delta_{\max}. \end{cases} \tag{4}$$

The volumetric depth calculated from the approximation (Equation 4) is compared (curve) with the direct calculation (Equation 3 (dots)) for four ice-wedge polygon in Figure 2 and representative of other polygons. Also, shown is the volumetric depth in the absence of microtopography, which is linear with slope unity. Equation 3 is a very good approximation.

3.2.2. Modified Flow law

Microtopographic effects on the flow law are not as straightforward to incorporate as the volumetric head $\Phi(\delta)$. In particular, we should make the distinction between depressions and obstractions [9]. Depressions are disconnected low points in the topography. The ponded depth must rise above the level of those depressions before any flow can happen. Obstructions exist above the depressions and interrupt and slow the flow, but do not block it completely. To model the effects of obstructions and depressions, we propose the following modification to the flow law

$$U = -\Theta(\delta) \frac{(\delta - \delta_{\text{d}})^{2/3}}{n_{\text{mann}}(\|\nabla Z\| + \epsilon)^{1/2}} \tag{5}$$

where δ_{d} is the depression depth, and $\Theta(\delta) \in [0,1]$ is a fractional conductance which account for flow reduction by obstructions. polygons-finescale

To calculate δ_{d} from the microtopography, we now propose an approach based on site percolation. Specifically, we fill the lowest elevation surface cells until the cluster of inundated cells spans the IWP. This is the percolation threshold. The water height at the percolation threshold defines the δ_{d}. Figure 3 shows the spanning cluster at the percolation threshold for the IWP C40 shown in Figure 4. The depression depth calculated this way is 4.1 cm for this IWP. It is reasonable to assume that the fractional conductance is well approximated by the fractional cross section available to flow, which can be estimated as the ratio of volumetric depth to ponded depth.

$$\Theta(\delta_{\mathrm{d}}) \approx \alpha \frac{(\Phi(\delta) - \Phi(\delta_{\mathrm{d}}))}{\delta} H\left(\delta - \delta_{\mathrm{d}}\right) \tag{6}$$

Where H is the Heaviside function and α is a drag factor to account for any additional resistance for flow [9]. The numerator is the flowing cross sectional area. Note the velocity is multiplied by ponded depth to get a flux, so the flux appearing in the conservation equations becomes

$$\delta U = -\alpha(\Phi(\delta) - \Phi(\delta_{\mathrm{d}}))H\left(\delta - \delta_{\mathrm{d}}\right) \frac{(\delta - \delta_{\mathrm{d}})^{2/3}}{n_{\mathrm{man}}(\|\nabla Z\| + \epsilon)^{1/2}} \nabla(Z + \delta) \tag{7}$$

In summary, we hypothesize that the microtopographic effects on surface flow can be captured with a simple approximation with three parameters that can be computed from the microtopography:

- Subgrid relief $\delta_{\max} = Z_{*,\max} - Z_{*,\min}$, where $Z_{*,\max}$ and $Z_{*,\min}$ are the maximum and minimum elevation in the microtopography.
- Specific excluded volume δ_{ex}, the soil volume above the microtopographic low point normalized by IWP area.

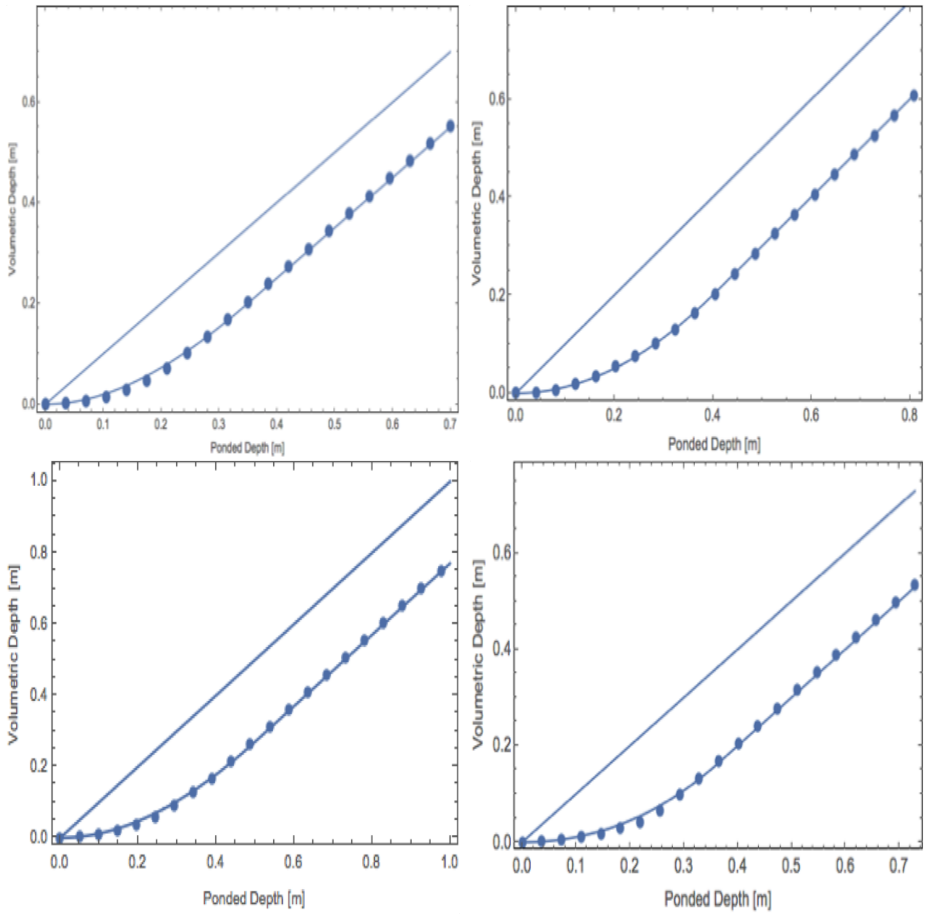

Figure 2: Volumetric depth versus ponded depth for four ice-wedge polygons. The ice-wedge polygons are displayed in Figure 4.

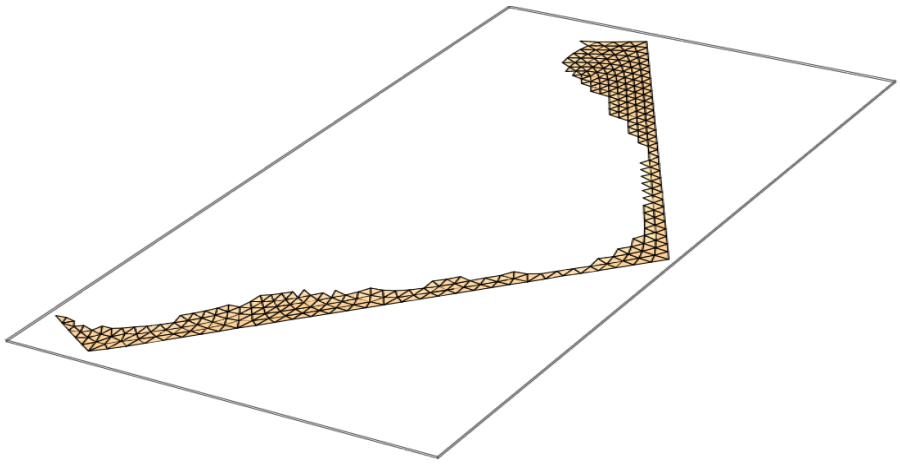

Figure 3: The spanning cluster at the percolation threshold for the IWP C40 (Figure 4). The water depth relative to the low point of the microtopography at the percolation threshold defines the depression depth.

- Depression depth δ, the difference between the maximum and minimum elevation of the cells in the spanning cluster at the percolation threshold.

The subgrid releif and specific excluded volume come directly from the microtopography (univariate statistics). The depression depth requires a simple percolation algorithm to identify the spanning cluster at the percolation threshold. Values are given in Table 2.

Table 2: Parameters used in the subgrid model

	C06	C31	C40	C44	C45	A0	B01
$\delta_{\max}(m)$	0.404	0.262	0.483	0.364	0.350	0.361	0.411
$\delta_{\mathrm{ex}}(m)$	0.2	0.105	0.23	0.2	0.15	0.185	0.26
$\delta_{\mathrm{d}}(m)$	0.069	0.128	0.043	0.187	0.164	0.222	0.143

4. The Advanced Terrestrial Simulator (ATS)

Here we provide a very brief overview of the ATS for a reference, for more details about the software infrastructure we refer the reader to [22, 23]. A fully integrated surface/subsurface and snow distribution modeling capability implemented in ATS are available here [7, 24]. In addition, a mixed-dimensional modeling strategy, mainly designed for the simulations of low-relief permafrost-affected regions, can be found here [3]. The ATS is a publically-available massively parallel computer code, an extended version of Amanzi (flow and reactive transport simulator; see [25]), based on process management tool called Arcos. In ATS, a proces kernel (PK) refers to governing mathematical equations representing a particular (or coupled) physical process(es). Further, Multiprocess Coordinators (MPCs) are available to facilitate coupling amoung PKs. The framework allows to dynamically build a complex/coupled hierarchical model structure. The flexible extensibility feature of the Arcos framework allowed to easily implement our subgrid model and couple with the existing PKs.

5. Numerical Results and Discussions

5.1. Simulations

To assess the accuracy of numerical results of our subgrid model, we compare our results with fine-scale simulations and a coarsened model without subgrid (hereinafter referred to as "no subgrid model"). For demonstration purpose, the comparison is made for surface-only flow simulations. In our work, the seven ice-wedge polygon for fine-scale simulations are considered

from Barrow Environmental Observatory (BEO) and illustrated in Figure 4. The ice-wedge polygons named A, B and C correspond to the NGEE Arctic field sites A, B and C (see Figure 1), respectively. Those polygons consist of low-centered, high-centered, with well established troughs (relatively uniform elevation across the trough) and obstructions in the troughs, and hence represent a broader class of polygonal landscape. Three sets of numerical experiments are performed with the subgrid model:

Study I: Evaluate the subgrid model with the parameters (uncalibrated) computed directly from surface microtopography;

Study II: Evaluate the subgrid model with calibrated values of the depression depth;

Study III: Evaluate the subgrid model with calibrated values of the depression depth and a drag coefficient. This is Study II with the inclusion of a drag factor in the flow law.

Study II is motivated by fine-scale simulations, higher depression depth may delay breakthrough, and would lead to more accumulation of water in the depressions. That said, in Study II we adjust the value the depression depth computed by the percolation algorithm to provide a better fit to the fine-scale results. The process of adjusting model's parameters to replicate the benchmark (e.g., fine-scale computational or real experiments) results is known as calibration. Moreover, higher pressure in the subgrid model affects the overland conductivity and hence the discharge rate. To mimic the behavior of the fine-scale at the time of breakthrough and recession period, the surface roughness is decreased by raising the manning coefficient in the governing equation. This analysis proposed Study III. Raising the manning coefficient is analogous to introducing a drag factor.

A pulse numerical test (injection followed by recession) is performed in the above mentioned three numerical studies. That is, we start with a fully dry surface, and inject water at a constant rate at the inlet boundary until breakthrough happens (prescribed flux boundary for a certain period of time), then stop the water supply and let water pass through the outlet (free drainage boundary). The inward and outward arrows shown in Figure 4 indicate the inlet and outlet boundaries. To point out, the entire fine-scale IWP is considered as one coarsened grid cell in the subgrid and no subgrid model – the elevation of faces depends on the elevation of the corners of the fine-scale IWP. It is important to mention that the higher (inlet) and lower (outlet) boundaries are chosen based on the average elevation of the faces in the coarsened grid. For instance, the inlet_2 in the coarsened grid of the polygon A01 (shown in Figure 4) is higher than the outlet_2, however, the fine-scale shows inlet_2 is lower than outlet_2.

The rainfall events are not considered in Studies I, II and III. The presence of a fixed depression depth parameter in the flow law of our subgrid model will not allow to replicate the shape of the hydrograph because the fine-scale simulations will show immediate breakthrough. To capture such a behavior it would be more practical to determine the value of the depression depth dynamicly – change the depression depth as the ponded depth changes. This sort of research will be reported somewhere else.

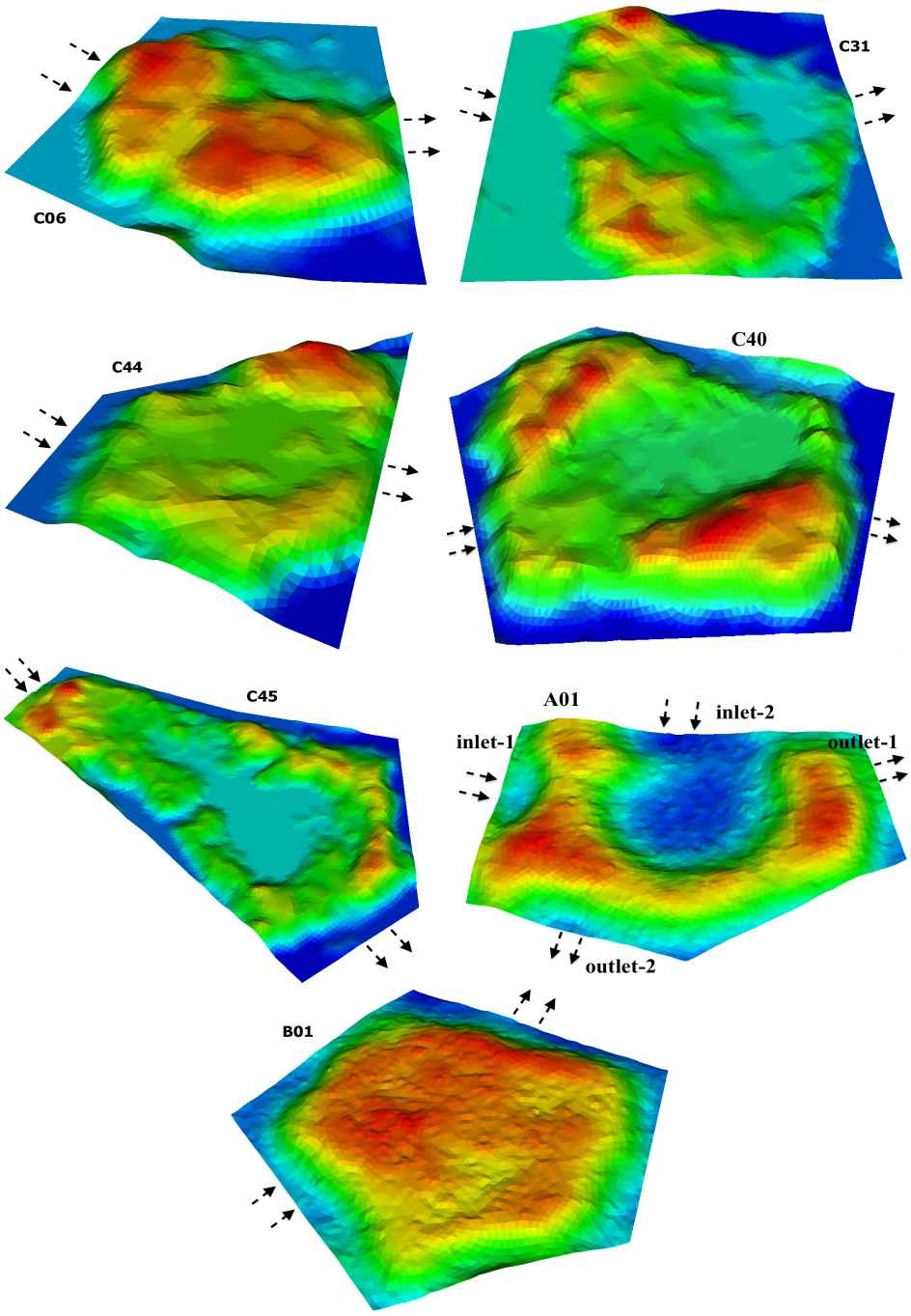

Figure 4: An Illustration of the microtopography of ice-wedge polygons from Barrow Environmental Observatory (BEO). Red and dark blue spots correspond to high- and low-elevated regions. The arrows indicate inlet and outlet boundaries.

5.2. Results and Discussions

Numerical results presented in this subsection correspond to the three studies mentioned above. We compare our results with fine-scale simulations of single IWPs, and we do not present any results on a cluster of fine-scale IWPs. We have carried out detailed simulations on all the polygons shown in Figure 4, however, we discuss the results of polygon C44 in more detail and these results serve as a representative of all the remaining polygons as far as the accuracy and shape of the hydrographs are concerned. Figure 5 compares the numerical results of the subgrid model with the fine-scale simulations, and no subgrid model of polygon C44. Clearly, Study I fails to match the fine-scale simulations, delayed breakthrough in the subgrid model is an indication of higher depression depth computed by the percolation algorithm; see Figure 5(a). Simulations with a calibrated depression depth, Study II, dramatically improve the shape of the hydragragh and the water content in the system as shown in see Figure 5(b). However, a mismatch appears at the time of breakthrough and the beginning of recession period even with the use of a calibrated depression depth. As alluded to earlier, this is due to the huge head gradient between the center and seepage face, and physically makes sense. Figure 5(c) illustrates the results of Study III, and it is evident that our subgrid model reproduces the fine-scale behavior, and the numerical results are identical to the fine-scale simulations. However, a complete mismatch is observed in numerical results of the no subgrid model.

Figure 6 compares the numerical results of Study I and III with the fine-scale and no subgrid model. The percolation algorithm computed the depression depth very accurately for polygon C06, and calibration (Study II) is not required. Similar to the results of polygon C44, the high overland conductivity in the subgrid model is reduced by increasing the surface

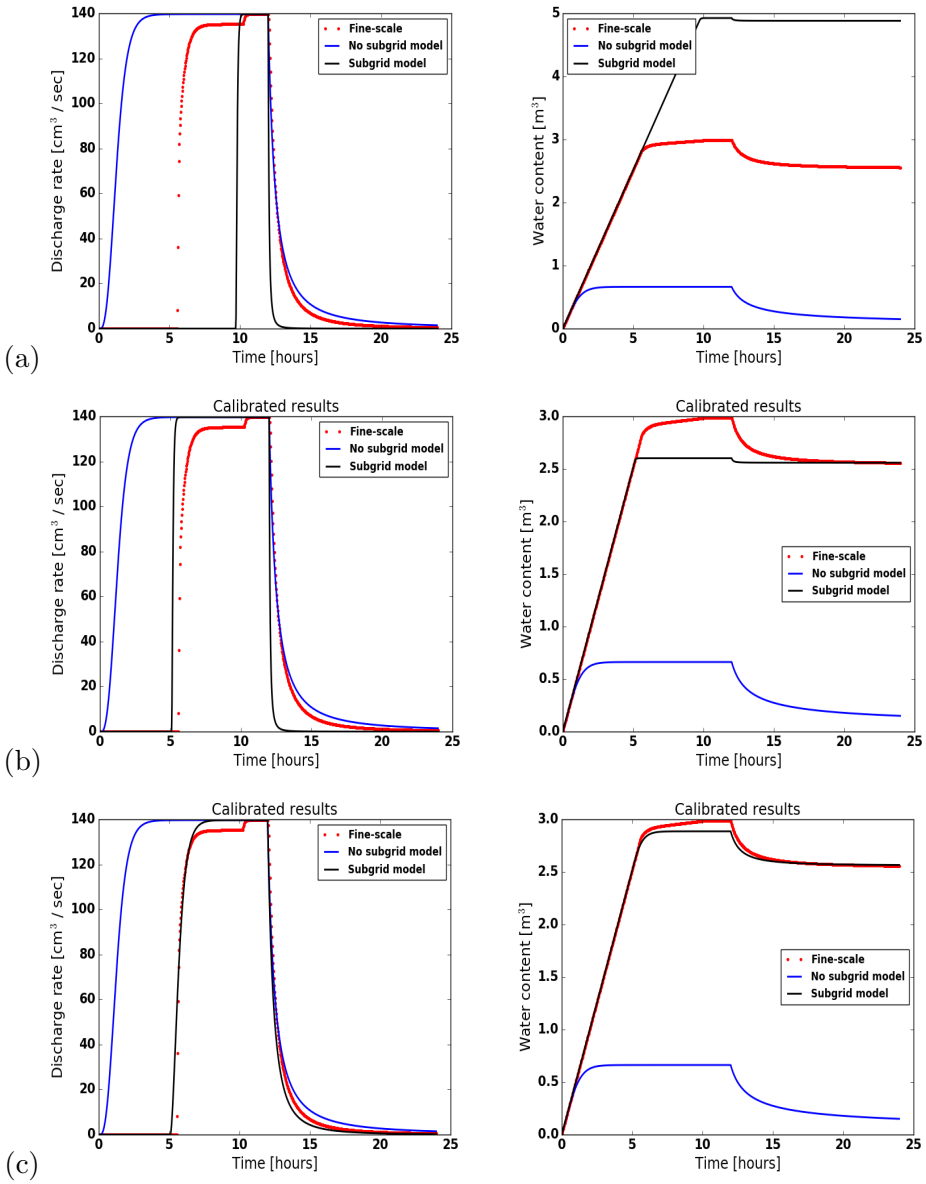

Figure 5: (Polygon C44) Comparison of the numerical results of the subgrid model with the fine-scale and no subgrid model results. Rows (top to bottom) correspond to Study I, II and III, respectively.

roughness. It improves the results and replicate the recession period of the fine-scale results. Figure 6 also displays the water retained in the subgrid and fine-scale models, the match is very close. For polygon C31, the results of the subgrid model are strongly affected by the depression depth in Study I, and lead to a mismatch. However, the results of Study II and III indicate that calibrated values of the depression depth and the surface roughness improved the simulated results dramatically and yield a close match as depicted in Figure 7. Numerical simulations correspond to polygons C40, C45, A01, and B01 are shown in Figures 8, 9, 10, and 11, respectively. In Figure 10, the results correspond to inlet_2 and outlet_2 boundaries, the results using inlet_1 and outlet_1 are discussed later in this subsection. Overall, the results of the subgrid model are very encouraging and consistently yield a better fit to the fine-scale results as compared to the no subgrid model.

5.3. Additional Remarks

- Not surprisingly, the subgrid model favors high surface roughness that swings the results toward fine-scale simulations. A high agreement between the results of the subgrid model and fine-scale simulations due to reduced runoff is an indication of a needed drag coefficient in the flow law. A linear regression fit to the drag factor vs. the depression depth is depicted in Figure 12. The drag factor varies between zero and one, as the depression depth decreases the drag factor goes to unity – a representation of flow over a flat surface. The fit indicates the resistance to flow increases with increasing depression. This finding is highly consistent with the discussion regarding the conductance terms in [9].

- For low-centered polygons such as C45 and A01, Study I (uncalibrated

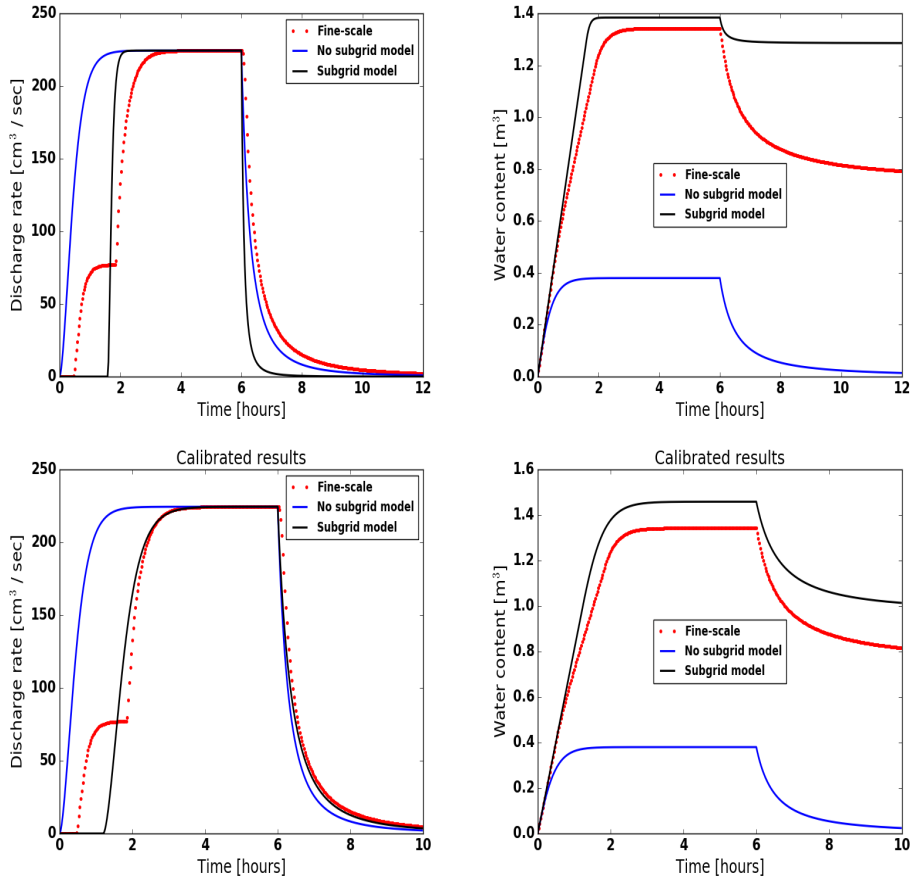

Figure 6: (Polygon C06) Comparison of the numerical results of the subgrid model with the fine-scale and without subgrid model results. Top and bottom row correspond to Study I and Study III, respectively.

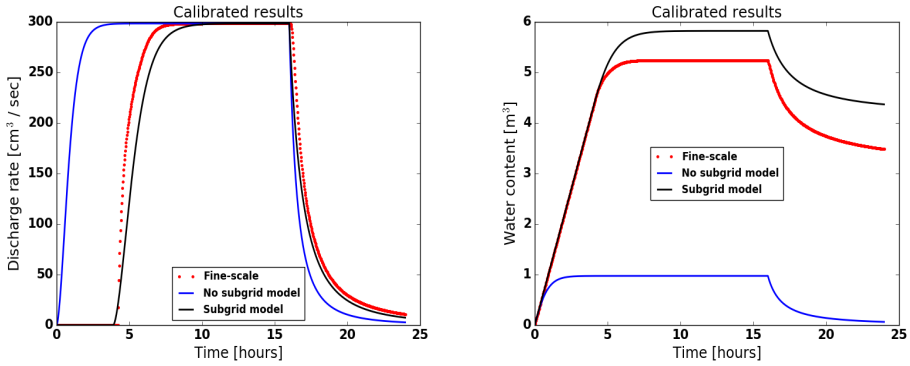

Figure 7: (Polygon C31) Comparison of the numerical results of the subgrid model with the fine-scale and no subgrid model. Results corresponded to Study III.

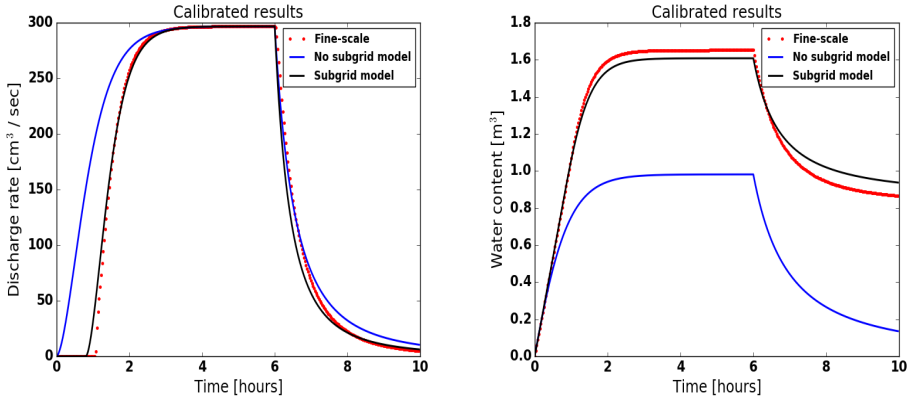

Figure 8: (Polygon C40) Comparison of the numerical results of the subgrid model with the fine-scale and without subgrid model results. Bottom row displays calibrated results.

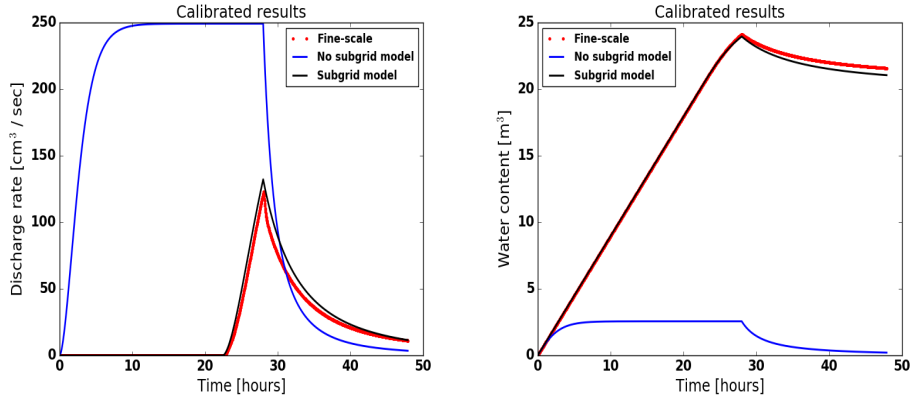

Figure 9: (Polygon C45) An illustration of the numerical results of the subgrid model, the fine-scale and no subgrid model. The simulations correspond to Study III.

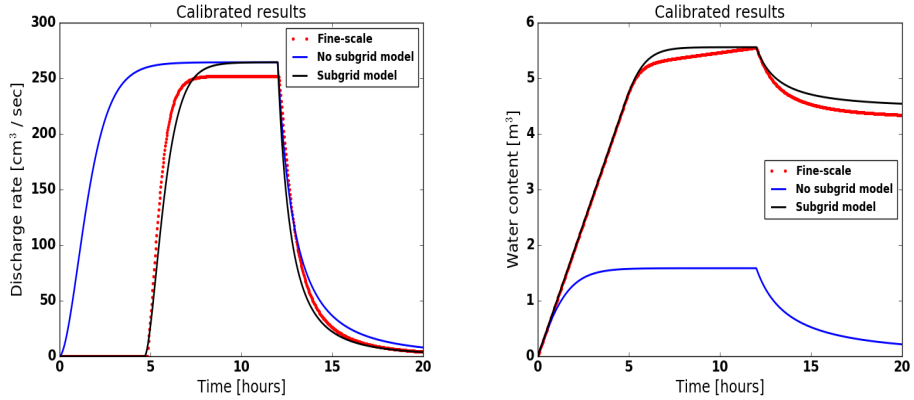

Figure 10: (Polygon A01) Comparison of the hydrographs and water content from the numerical simulation of the fine-scale, subgrid and no subgrid models. The results correspond to inlet_2 and outlet_2 boundaries.

results) fails to match the hydrograph of the fine-scale simulations – no breakthrough happens if uncalibrated depression depths are used. Fine-scale simulations show that low-elevated regions may remain completely dry if they are not located in the main flow channel which is trivial. However, as stated earlier, our percolation algorithm fills the

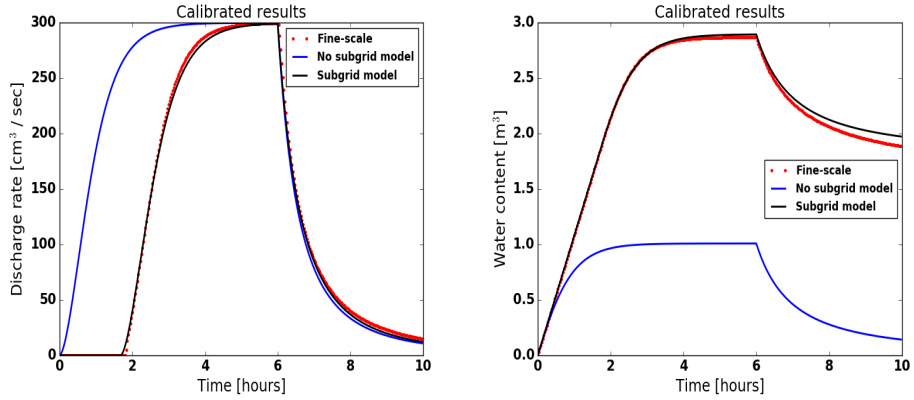

Figure 11: (Polygon B01) Comparison of the numerical results of the subgrid model with the fine-scale and without subgrid model results.

lowest elevation cells until the cluster of inundated cells spans the IWP. Thereby, the direction of the injected fluid is important. For instance, considering polygon A01, the results are not comparable if the inlet and outlet are at sides inlet_1 and outlet_1, respectively. However, if the inlet and outlet are switched to inlet_2 and outlet_2 a desirable match is obtained; see Figure 13.

- An empirical relation correlating the uncalibrated (directly measured from the microtopographic data) and calibrated (insight from fine-scale simulations to adjust the uncalibrated values) depression depths is shown in Figure 12. The fitted curve with the coefficient of determination 0.82 yields a good match. As a subject for future research, the application of invaded percolation (flow in the direction of least resistance) algorithm could provide more accurate depression depths, and would probably overcome the issues of calibrating parameters and/or location of inlet and outlet boundaries.

- Most of our numerical experiments show that the subgrid model outperforms the no subgrid model even when the fine-scale flow behavior is not completely captured.

- When the inlet boundary has obstructions (for example, polygon C06 in Figure 4) and divides the incoming water into different flow channels, the water reaches the outlet boundary at different times and lead to a dual-peak (or may be multiple-peak) hydrograph. Due to only one grid cell in the subgrid model, the dual-peak behavior is not possible to capture.

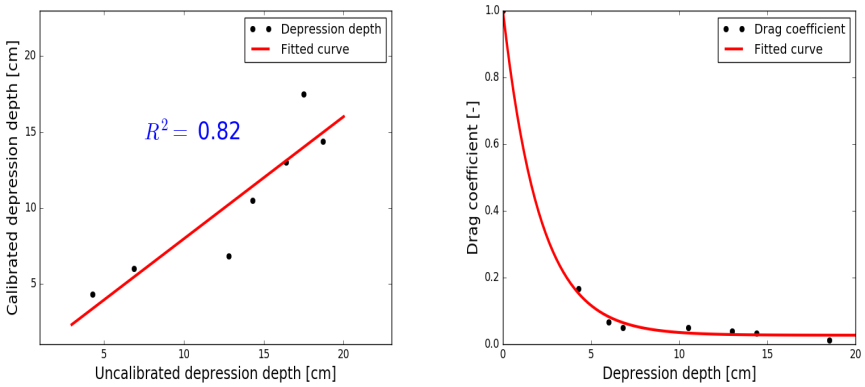

Figure 12: (Left) Linear fitted-curve to the depression depth data. (Right) Drag factor vs. calibrated depression depth.

6. Conclusions

The subgrid model presented in this paper is aimed at incorporating the microtopographic effects in the governing equations for the simulations of integrated surface/subsurface processes at watershed-scale.

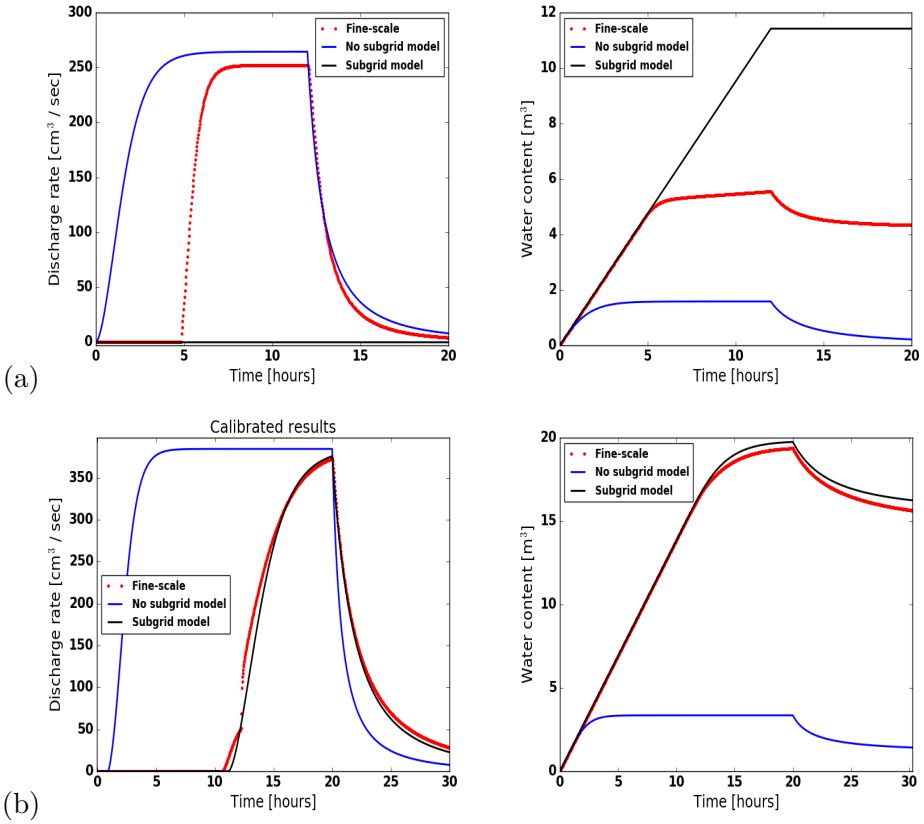

Figure 13: (Polygon A01) An illustration of the numerical results based on the choice of the inlet and outlet boundaries. The orientation affects the match between the fine-scale and subgrid model. (a) inlet_1 and outlet_1 boundary; (b) inlet_2 and outlet_2 boundary.

Standalone fine-scale surface simulations are tractable with the existing sophisticated computing tools. However, a significant challenge is how to capture accurate flow behavior in the watershed-scale integrated models because fine-scale simulations of integrated models at such a scale are not feasible. Seven fine-scale ice-wedge polygons are considered to demonstrate that the effect of surface microtopography can be captured in coarsened models through the use of a subgrid

model. Numerical results of the subgrid model compare very well with the fine-scale simulations. Our analysis shows that accurate estimate of depression depth is a determining factor for a close match between subgrid and fine-scale simulations. Three different studies are conducted to estimate the parameters: (1) direct measurements from topography; (2) insight from fine-scale simulations to calibrate; (3) and empirical adjustment of topography-derived values. Thus the effort to obtain a reasonable match with the fine-scale simulations using coarsened meshes with a subgrid representation was highly successful. The model is applied to 468 polygons watershed and a comparison is made no subgrid model. Numerical results demonstrate the importance of microtopography effects in watershed-scale simulations. **(this part will change once we add 486 polygons results)**. The subgrid model's ability to accurately capture fine-scale flow behavior provides confidence that a few parameters extracted from the available microtopographic data can be used to incorporate the fine-scale effects in watershed-scale integrated models. However, more research is needed to extend the approach developed here to accurately simulate problems involving both runoff and precipitation.

References

[1] J.-K. Huang, K. T. Lee, Influences of spatially heterogeneous roughness on flow hydrographs, Advances in water resources 32 (2009) 1580–1587.

[2] C. G. Andresen, V. L. Lougheed, Disappearing arctic tundra ponds: Fine-scale analysis of surface hydrology in drained thaw

lake basins over a 65 year period (1948–2013), Journal of Geophysical Research: Biogeosciences 120 (2015) 466–479.

[3] A. Jan, E. T. Coon, P. S. L., R. Garimella, J. D. Moulton, An intermediate-scale model for thermal hydrology in low-relief permafrost-affected landscapes, Submitted to Computational Geosciences (2016).

[4] J. Holden, Peatland hydrology and carbon release: why small-scale process matters, Philosophical Transactions of the Royal Society of London A: Mathematical, Physical and Engineering Sciences 363 (2005) 2891–2913.

[5] S. Painter, J. Moulton, C. Wilson, Modeling challenges for predicting hydrologic response to degrading permafrost, Hydrogeology Journal (2013) 1–4.

[6] B. L. Kurylyk, K. T. MacQuarrie, J. M. McKenzie, Climate change impacts on groundwater and soil temperatures in cold and temperate regions: Implications, mathematical theory, and emerging simulation tools, Earth-Science Reviews 138 (2014) 313–334.

[7] S. L. Painter, E. T. Coon, A. L. Atchley, M. Berndt, R. Garimella, J. D. Moulton, D. Svyatskiy, C. J. Wilson, Integrated surface/subsurface permafrost thermal hydrology: Model formulation and proof-of-concept simulations, Water Resources Research 52 (2016) 6062–6077.

[8] W. N. Stammers, H. Ayers, The effect of slope and microtopog-

raphy on depression storage and surface detention, publisher not identified, 1956.

[9] S. Panday, P. S. Huyakorn, A fully coupled physically-based spatially-distributed model for evaluating surface/subsurface flow, Advances in water Resources 27 (2004) 361–382.

[10] E. A. G. Schuur, A. D. McGuire, C. Schaedel, G. Grosse, J. W. Harden, D. J. Hayes, G. Hugelius, C. D. Koven, P. Kuhry, D. M. Lawrence, S. M. Natali, D. Olefeldt, V. E. Romanovsky, K. Schaefer, M. R. Turetsky, C. C. Treat, J. E. Vonk, Climate change and the permafrost carbon feedback, NATURE 520 (2015) 171–179.

[11] G. Hugelius, J. Strauss, S. Zubrzycki, J. W. Harden, E. A. G. Schuur, C.-L. Ping, L. Schirrmeister, G. Grosse, G. J. Michaelson, C. D. Koven, J. A. O'Donnell, B. Elberling, U. Mishra, P. Camill, Z. Yu, J. Palmtag, P. Kuhry, Estimated stocks of circumpolar permafrost carbon with quantified uncertainty ranges and identified data gaps, Biogeosciences 11 (2014) 6573–6593.

[12] L. D. Hinzman, N. D. Bettez, W. R. Bolton, F. S. Chapin, M. B. Dyurgerov, C. L. Fastie, B. Griffith, R. D. Hollister, A. Hope, H. P. Huntington, et al., Evidence and implications of recent climate change in northern alaska and other arctic regions, Climatic Change 72 (2005) 251–298.

[13] A. H. Lachenbruch, Mechanics of thermal contraction cracks and ice-wedge polygons in permafrost, Geological Society of America Special Papers 70 (1962) 1–66.

[14] G. W. Greene, Contraction theory of ice-wedge polygons: A qualitative discussion, 1963.

[15] J. R. Mackay, Some observations on the growth and deformation of epigenetic, syngenetic and anti-syngenetic ice wedges, Permafrost and Periglacial Processes 1 (1990) 15–29.

[16] J. Mackay, Thermally induced movements in ice-wedge polygons, western arctic coast, Geomorphology: Critical Concepts in Geography 5 (2004) 477.

[17] J. Kumar, N. Collier, G. Bisht, R. T. Mills, P. E. Thornton, C. M. Iversen, V. Romanovsky, Modeling the spatiotemporal variability in subsurface thermal regimes across a low-relief polygonal tundra landscape, The Cryosphere 10 (2016) 2241–2274.

[18] M. T. Jorgenson, Y. L. Shur, E. R. Pullman, Abrupt increase in permafrost degradation in arctic alaska, Geophysical Research Letters 33 (2006).

[19] A. K. Liljedahl, J. Boike, R. P. Daanen, A. N. Fedorov, G. V. Frost, G. Grosse, L. D. Hinzman, Y. Iijma, J. C. Jorgenson, N. Matveyeva, et al., Pan-arctic ice-wedge degradation in warming permafrost and its influence on tundra hydrology, Nature Geoscience (2016).

[20] J. C. Rowland, C. E. Jones, G. Altmann, R. Bryan, B. T. Crosby, L. D. Hinzman, D. L. Kane, D. M. Lawrence, A. Mancino, P. Marsh, J. P. McNamara, V. E. Romanvosky, H. Toniolo, B. J. Travis, E. Trochim, C. J. Wilson, G. L. Geernaert, Arctic

landscapes in transition: Responses to thawing permafrost, Eos, Transactions American Geophysical Union 91 (2010) 229–230.

[21] A. Liljedahl, L. Hinzman, J. Schulla, Ice-wedge polygon type controls low-gradient watershed-scale hydrology, in: Proceedings of the Tenth International Conference on Permafrost, volume 1, 2012, pp. 231–236.

[22] E. T. Coon, J. D. Moulton, S. L. Painter, Managing complexity in simulations of land surface and near-surface processes, Water Resources Research 78 (2016) 134–149.

[23] E. T. Coon, ATS: The Advanced Terrestrial Simulator, 2016. http://github.com/amanzi/ats.

[24] A. L. Atchley, S. L. Painter, D. R. Harp, E. T. Coon, C. J. Wilson, A. K. Liljedahl, V. E. Romanovsky, Using field observations to inform thermal hydrology models of permafrost dynamics with ats (v0.83), Geoscientific Model Development 8 (2015) 2701–2722.

[25] J. D. Moulton, M. Berndt, R. Garimella, L. Prichett-Sheats, G. Hammond, M. Day, J. Meza, High-level design of amanzi, the multi-process high performance computing simulator, office of environmental management, united states department of energy, washington dc (2012).